Configurational entropy of binary hard-disk glasses: Nonexistence of an ideal glass transition

Aleksandar Donev
Program in Applied and Computational Mathematics, Princeton University, Princeton, New Jersey 08544, USA and Princeton Institute for the Science and Technology of Materials, Princeton University, Princeton, New Jersey 08544, USA

Frank H. Stillinger
Department of Chemistry, Princeton University, Princeton, New Jersey 08544, USA

Salvatore Torquato[a)]
Department of Chemistry, Princeton University, Princeton, New Jersey 08544, USA, Program in Applied and Computational Mathematics, Princeton University, Princeton, New Jersey 08544, USA, Princeton Institute for the Science and Technology of Materials, Princeton University, Princeton, New Jersey 08544, USA and Princeton Center for Theoretical Physics, Princeton University, Princeton, New Jersey 08544, USA

(Received 5 April 2007; accepted 2 August 2007; published online 28 September 2007)

We study the thermodynamics of a binary hard-disk mixture in which the ratio of disk diameters is $\kappa=1.4$. We use a recently developed molecular dynamics algorithm to calculate the free-volume entropy of glassy configurations and obtain the configurational entropy (degeneracy) of the supercompressed liquid as a function of density. We find that the configurational entropy of the glasses near the kinetic glass transition is very close to the mixing entropy, suggesting that the degeneracy is zero only for the phase-separated crystal. We explicitly construct an exponential number of jammed packings with densities spanning the spectrum from the accepted "amorphous" glassy state to the phase-separated crystal, thus showing that there is no ideal glass transition in binary hard-disk mixtures. This construction also demonstrates that the ideal glass, defined as having zero configurational entropy, is not amorphous, but instead is nothing more than a phase-separated crystal. This critique of the presumed existence of an ideal glass parallels our previous critique of the idea that there is a most-dense random (close) packing for hard spheres [Torquato *et al.*, Phys. Rev. Lett. **84**, 2064 (2000)]. We also perform free-energy calculations to determine the equilibrium phase behavior of the system. The calculations predict a first-order freezing transition at a density below the kinetic glass transition. However, this transition appears to be strongly kinetically suppressed and is not observed directly. New simulation techniques are needed in order to gain a more complete understanding of the thermodynamic and kinetic behavior of the binary disk mixture and, in particular, of the demixing process during crystallization. © *2007 American Institute of Physics*. [DOI: 10.1063/1.2775928]

I. INTRODUCTION

One of the outstanding challenges of condensed matter physics remains to be the understanding the glass transition in dense or supercooled liquids.[1–3] Numerous efforts have been made to identify the cause of the dramatic slowdown of the dynamics (specifically, the decrease of the diffusion coefficient and the increase in relaxation times) in the vicinity of the *kinetic glass transition*. A popular hypothesis has been that a thermodynamic transition distinct from the usual liquid-solid transition underlies the kinetic glass transition. Adam and Gibbs first proposed[4] a scenario that relates the slow diffusion to a vanishing of the number of alternative configurations available to the liquid. In this scenario, an *ideal thermodynamic* glass transition occurs when the liquid remains trapped in one of the few remaining glassy configurations.[5,6] These ideal glass theories make the basic assumption that the thermodynamically favored crystalline configurations are kinetically inaccessible and, therefore, the liquid is restricted to exploring "amorphous" configurations, qualitatively different from crystal ones.

In this paper, we study a specific prototypical glass former, namely, a binary hard-disk mixture with size ratio of 1.4. For this model, we show that there is no special amorphous (random) state, but rather a continuum of states from the most disordered one ("maximally random jammed" state) to the most ordered one.[7] In fact, we find that the presumed "ideal glass" is nothing more than a phase-separated crystal! We believe that the conclusions drawn in this paper for the binary hard-disk system generalize to other structural glass formers, such as mono- and bidisperse with hard-core and soft interactions, as we will discuss in Sec. V.

Before we present our new results, we give some relevant background information. In Sec. II A, we compare the thermodynamics of hard-particle systems to the more familiar thermodynamics of soft-particle systems, and describe the

[a)]Electronic mail: torquato@electron.princeton.edu

TABLE I. A comparison of analogous concepts between soft- and hard-particle systems. Decreasing a quantity is indicated via ↓, and increasing it via ↑. Question marks indicate an open question.

Soft	Hard	Notes
$T\downarrow$	$p\uparrow$	State control variable
$T\downarrow$	$\phi\uparrow$	Alternative state control
Cooling rate ↓	Particle growth rate $\gamma\downarrow$	Quenching speed
Inherent structure	Jammed packing	Exact[a] in limit $p\to 0$
Basin depth $U_{\mathrm{IS}}\downarrow$	Jamming density $\phi_J\uparrow$	Quench rate ↓
Vibrational FE $f_{\mathrm{vib}}^{\mathrm{IS}}$	Free-volume FE $f_g\sim -\ln V_{FV}$	Exact[b] in limit $T\to 0$ or $\phi\to\phi_J$
Saddle point	Unstable packing [?]	Saddle index[c] $x\equiv(M-Nd)/N$
Barrier height ↑	Channel width ↓ [?]	Not well understood[d]

[a]References 13 and 14.
[b]Reference 25.
[c]Reference 15.
[d]Reference 16.

molecular dynamics (MD) algorithm used to obtain equilibrated dense liquid states and to produce binary hard-disk jammed packings and glasses. In Sec. II B, we will review the inherent-structure formalism for dense liquids, as specialized for hard-particle systems, and sketch a theory proposing that a thermodynamic ideal glass transition underlies the experimentally and computationally observed kinetic transition. In Sec. II C, we briefly review the MD algorithm used to measure the free-volume contribution to the free energy for hard-sphere systems. Our results for the equilibrium thermodynamic properties of a hard-disk mixture are presented in Sec. III. Nonequilibrium glasses are considered in Sec. IV, and some concluding remarks are offered in Sec. V. Some of the results from the work presented here were previously reported in a brief letter.[8] Here, we expand on theoretical and computational details and report additional new results.

II. BACKGROUND

Hard-particle systems are athermal, in the sense that the derivatives of the configurational partition function are independent of the temperature T. Therefore, apart from a trivial scaling with temperature, the thermodynamic properties are solely a function of the *density* (volume fraction) ϕ.[9] One must consider a hard-particle system at a positive temperature (we fix $k_BT=1$), since the free-energy (FE) of the hard-sphere system consists entirely of the entropic term, $F=-TS$. At positive temperature, the time-averaged thermal motion of the particles leads to a well-defined free energy and its derivatives with respect to strain, i.e., stress and elastic moduli (bulk and shear moduli for isotropic states), exist just as for soft-particle systems. For soft-particle systems, the limit $T\to 0$ is thermodynamically well defined, and in that limit the free energy becomes equal to just the potential energy $F=U$.

In Table I we give a comparison between hard- and soft-particle systems for some of the main quantities used in thermodynamic considerations of glasses. Some of the hard-particle quantities in this table are defined more precisely in later sections. Temperature is the primary state control variable for soft-particle systems, and decreasing the temperature is equivalent to increasing the density or pressure in hard-sphere systems. Upon cooling to zero temperature, soft-particle systems go into states of minimal potential energy. The energy minima, or inherent structures,[10] for certain soft-particle systems, in the limit of zero pressure (i.e., zero internal stress), correspond to (collectively) *jammed packings*,[11,12] which are mechanically stable packings where the particles are trapped in a static configuration despite thermal or external agitation.[13,14] Upon reducing the quench (cooling or compression) rate, the final inherent structures reach deeper basins (wells) of the energy landscape, as measured by the depth of the energy minimum U_{IS}. The width of the basins can be quantified via the vibrational free energy $f_{\mathrm{vib}}^{\mathrm{IS}}$ (as calculated in the harmonic approximation). At sufficiently low temperatures, the transitions between nearby basins pass through saddle points of low saddle index,[15] and the frequency of transitions is determined by the barrier height (difference in potential energy between the saddle point and the starting inherent structure). Since hard-particle systems have trivial internal energy, it is not obvious how to relate to soft-particle concepts of saddle points and energy barriers; however, some ideas are discussed in Ref. 16.

A. Thermodynamics of nearly jammed hard-particle systems

We produce jammed packings in d dimensions by using the Lubachevsky-Stillinger MD algorithm.[17,18] Small particles of diameter D are randomly distributed and randomly oriented in a box with periodic boundary conditions and without any overlap. The particles are given (linear and angular) velocities and their motion followed as they collide elastically and also expand uniformly (i.e., preserving their shape) at a certain *growth* or *expansion rate* $\gamma=dD/dt$, using a collision-driven MD algorithm.[19] Asymptotically, as the density increases, a *jammed packing* with a diverging collision rate and (locally) maximal *jamming density* ϕ_J is reached. Intuitively, a jammed (compactly packed, mechanically stable) packing is one where the particles are locked in their positions despite thermal agitation (shaking) and, potentially, boundary deformations (external loading). The number of contacts (constraints) M in such packings is typically equal to the total number of degrees of freedom, $M\approx Nd$, where N is the number of particles.[20] Depending on the boundary conditions and whether collective particle rear-

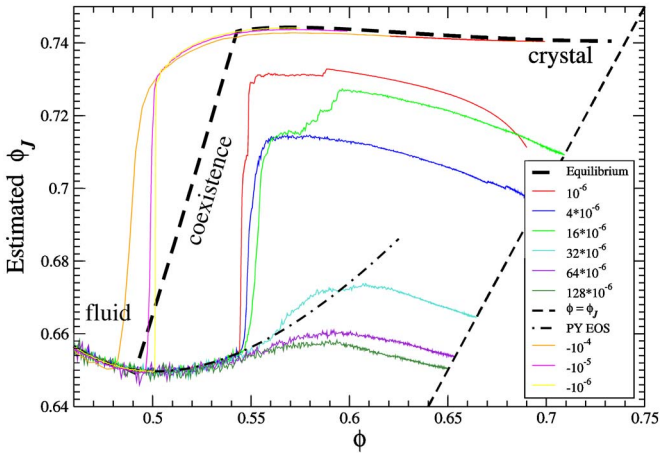

FIG. 1. (Color online) The estimated jamming packing fraction $\tilde{\phi}_J$ as a function of packing fraction ϕ for $d=3$, as produced by our (modified Lubachevsky-Stillinger) MD algorithm. Shown are systems of 4096 spheres with various expansion rates, showing the crystallization that occurs for sufficiently slow particle expansion and the kinetic glass transition for fast particle expansion, leading to disordered packings. Also shown are results for systems of 10 976 spheres placed in an fcc lattice with negative expansion rates (last three curves). For comparison, we plot approximations to the equilibrium EOS for the fluid phase, the coexistence region, and the crystal phase (Refs. 65 and 66), as well as the Percus-Yevick (PY) EOS (Ref. 67) for the fluid phase.

rangements take place, one can define different jamming categories, organized hierarchically into *local*, *collective*, and *strict* jamming in Ref. 21. The algorithm never reaches the true jammed state, and the particles have some *free volume* V_{FV} to rattle within which shrinks as the reduced *pressure* $p=PV/Nk_BT$ diverges.

Next, we briefly illustrate how the behavior of the LS algorithm is related to the thermodynamic properties of the system, for the familiar hard-sphere system in three dimensions. In Fig. 1, we show the *equation of state* (EOS) of a hard-sphere system as the density is increased slowly, through the growth of particles at an expansion rate γ, starting from a liquid. The pressure of the system is measured in the MD algorithm by averaging over a time period that is as small as possible but sufficiently large to average over many collisions. Instead of plotting the reduced pressure p directly, we use the well-known fact that near jamming the reduced pressure is asymptotically given by the free-volume equation of state,[22]

$$p=\frac{PV}{Nk_BT}\approx\frac{d}{1-\phi/\phi_J}, \tag{1}$$

which can be inverted to give an estimate $\tilde{\phi}_J$ of the jamming density,

$$\tilde{\phi}_J=\frac{\phi}{1-d/p}. \tag{2}$$

Since the pressure increases very rapidly near jamming, it is more convenient to plot the estimated jamming density $\tilde{\phi}_J(\phi)$ instead of the pressure $p(\phi)$, and we do this in Fig. 1 for several different expansion rates. The particles can also shrink ($\gamma<0$) starting from a dense configuration such as the FCC crystal, in which case the EOS along the crystal branch can be obtained for densities ranging from the crystal jamming density to the freezing density $\phi\approx0.50$. We note that the results in Fig. 1 are new and presented here for the first time.

In the limit $\gamma\to0$ (and $N\to\infty$), we obtain the thermodynamic equilibrium behavior of the hard-sphere system, and for small enough γ, the system is in quasiequilibrium, in the sense that the rate of density change is slow enough to allow for full relaxation of the system. For finite γ, the system is not in true equilibrium, and, in fact, as the relaxation time of the liquid grows due to the increase in density and increased proximity to jamming, the system may become trapped in a glassy state. This is exactly what is observed in Fig. 1. For small γ, there is a first-order transition from the liquid to the crystal branch around the melting point $\phi\approx0.55$. However, for larger γ, there is a kinetic glass transition around $\phi\approx0.6$ leading to nonequilibrium glassy states that eventually produce random jammed packings with jamming density $\phi_J\approx0.64$. If the expansion rate is intermediate, *partial crystallization* occurs leading to the formation of small nucleated crystallites inside a random packing matrix, or the formed polycrystal can be distorted and have multiple grain boundaries between crystallites with different orientations.

In light of the observations presented in Fig. 1, we see that it is not possible to extend the thermodynamic liquid branch beyond the melting point in a well-defined manner in the *absence of constraints*. Fast compressions suppress crystallization; however, these configurations are also clearly not in any kind of (local or metastable) equilibrium, since the observed EOS depends strongly on the exact value of γ above the melting point. Slowing the compression sufficiently to obtain a reproducible EOS leads to partial crystallization at densities above the melting point (crystallization does not occur at the freezing point as expected based on thermodynamic consideration because of finite-size effects). This is the reason why we have used binary hard disks in this study instead of using monodisperse hard spheres. As we will see in Sec. IV A, for a certain binary disk mixture, we are able to obtain an apparently well-defined liquid EOS up to the kinetic glass transition density.

It should be noted that one can create metastable states above the freezing point by imposing constraints. For example, Rintoul and Torquato[23,24] generated constrained metastable monodispersed hard-sphere systems above the freezing point by excluding those configurations in which the value of the bond-orientational order parameter was above a certain threshold value. Importantly, it was shown that such amorphous systems crystallized after sufficiently long times, i.e., there was no evidence of a glass transition of thermodynamic origin.

B. Inherent-structure thermodynamic formalism

Stillinger and Weber proposed an inherent-structure formalism that has since been used extensively in the analysis of the thermodynamics of supercooled liquids.[5,6,10] For systems of soft particles a central quantity in this thermodynamic formalism is the number of distinct energy minima (basins) with a given energy per particle. For hard-particle

systems, this quantity translates to the number of distinct jammed packings $N_g(\phi_J)=\exp[Ns_c(\phi_J)]$ with jamming packing fraction (density) ϕ_J, where $s_c(\phi_J)$ is the *configurational entropy*, or *degeneracy*, per particle. (The dimensionless quantity s_c is actually the conventional entropy divided by Boltzmann's constant. However, we will refer to it simply as "entropy" for convenience.) The formalism assumes that the liquid performs infrequent jumps from one basin to another as it explores the available configuration space, remaining in the vicinity of these jamming basins for long periods of time. Free-volume terms in the free energy favor denser packings, and, therefore, the basin belonging to the densest crystal, with density $\phi_{\max}$, is most favored. However, it is reasonable to assume that the degeneracy contribution to the free energy $s_c(\phi_J)$ decreases with increasing ϕ_J, favoring less dense but more numerous configurations. The liquid trades off degeneracy for free volume and, at a given density ϕ, it predominantly samples glasses with jamming density $\hat{\phi}_J(\phi)$, which have the lowest total free energy. The theory of cooperatively rearranging regions developed by Adam and Gibbs[4] proposes that the structural relaxation time in the metastable liquid is on the order of

$$\tau(\phi) \sim \exp\left\{\frac{C}{Ts_c[\hat{\phi}_J(\phi)]}\right\},$$

and, therefore, diverges at the ideal glass transition, where s_c vanishes.

We can approximate the free-volume contribution to the free energy (per particle) of a glass f_g close to the jamming point by integrating Eq. (1) to obtain

$$f_g(\phi,\phi_J) = -d\ln\left(1-\frac{\phi}{\phi_J}\right) - f_J(\phi_J),$$

where the term f_J depends on the structure of the jammed packing.[25] The (total) volume of configuration space corresponding to jamming density ϕ_J is a sum over all of the $s_c(\phi_J)$ basins, and therefore the contribution to the free energy from the glasses with jamming density ϕ_J is approximately

$$f(\phi,\phi_J) = f_g(\phi,\phi_J) + s_c(\phi_J).$$

At a given density ϕ, the jamming density that maximizes f is the one that dominates the thermodynamic integrals, and it is found from the solution $\hat{\phi}_J(\phi)$ of the equation

$$\left.\frac{\partial f}{\partial \phi_J}\right|_{\phi_J=\hat{\phi}_J(\phi)} = \left[-\frac{d}{\phi(1-\phi/\phi_J)} - \frac{\partial f_J(\phi_J)}{\partial \phi_J} + \frac{\partial s_c(\phi_J)}{\partial \phi_J}\right]_{\phi_J=\hat{\phi}_J(\phi)} = 0. \quad (3)$$

As expected, the pressure of the metastable glass is equal to the pressure of just one of the jamming basins and is not affected by the fact that the packing explores multiple (statistically identical) basins,

$$p = \phi\frac{df}{d\phi} = \phi\frac{\partial f}{\partial \phi_J}\frac{\partial \phi_J}{\partial \phi} + \phi\frac{\partial f}{\partial \phi} = \phi\frac{\partial f}{\partial \phi} = \frac{d}{(1-\phi/\phi_J)}.$$

The configurational entropy $s_c(\phi_J)$ must vanish above some density $\phi_J^{\max}$, if nothing else than because $\phi_J^{\max} \leqslant \phi_{\max}=\pi/\sqrt{18}$. The conjectured *ideal glass state* corresponds to the point where the number of available basins becomes subexponential, that is, $s_c(\phi_J^{\mathrm{IG}})=0$. The usual assumption in the literature is that $s_c(\phi_J)$ is an inverted parabola and that f_J is constant, and this assumption gives a monotonically increasing $\hat{\phi}_J(\phi)$.[6,26,27] The liquid becomes permanently trapped in the ideal glass state at densities above an ideal glass transition density ϕ_{IG}, defined via $\hat{\phi}_J(\phi_{\mathrm{IG}})=\phi_J^{\mathrm{IG}}$. A crucial unquestioned assumption has been that there is a gap in the density of jammed states between the amorphous and crystal ones, so that $\phi_J^{\mathrm{IG}}<\phi_{\max}$. In Sec. IV we will explicitly show that this assumption is flawed for the binary hard-disk mixture we study, and suggest that this is the case in other similar models, contrary to numerous estimates for ϕ_J^{IG} in the literature.[27–32]

C. BCMD free-energy algorithm

In Ref. 25, we present in detail our bounding cell molecular dynamics (BCMD) algorithm for computing the free energy (equivalently, entropy) of nearly jammed hard-particle packings, i.e., hard-particle systems where diffusion can be ignored and particles remain localized in the vicinity of their initial configuration for long times. Note that (nearly) jammed packings are not in thermodynamic equilibrium and, therefore, the free energy we calculate is not the equilibrium free energy at the given packing fraction (density), but rather, it is the free-volume contribution f_g to the thermodynamic free energy. Formally, the algorithm measures the true thermodynamic entropy of a single-occupancy cell (SOC) system;[33] however, with cells that are not complex polyhedra and which do not necessarily cover space. Namely, each particle is surrounded by a hard-wall *bounding cell* which has exactly the same shape as the particle itself, but is scaled uniformly by a scaling factor $\mu=1+\Delta\mu$. A slight modification of the algorithm in Ref. 19 keeps each particle within its bounding cell by predicting and processing collisions between the particles and the cell walls.

We focus on solidlike systems, meaning that there is no or very little free diffusion, so that over long periods of time the particles do not move far away from their initial positions (i.e., the centers of the cells). When the cells are very large, that is, $\mu=\mu_{\max}\gg 1$, the SOC system is virtually indistinguishable in its thermodynamic properties from the unconstrained system. In the limit $\mu\to 1$, the cells will become disjoint and the system becomes a collection of N independent particles, which can be treated analytically. We will assume that there exists a $\mu_{\min}>1$ for which the cells are fully disjoint. This can always be assured by preparing the initial state more carefully or by shrinking the particles slightly. During the course of the MD, we can measure the average reduced pressure on the walls of a cell $p_c=P_cV_c/k_BT$ and then obtain the change in free energy as the work done in shrinking the cells by integrating p_c. This gives the free energy of the SOC system with cells of size $\mu_{\max}$, which is a good approximation to f_g for sufficiently dense configurations. If the particles can diffuse freely given sufficient time

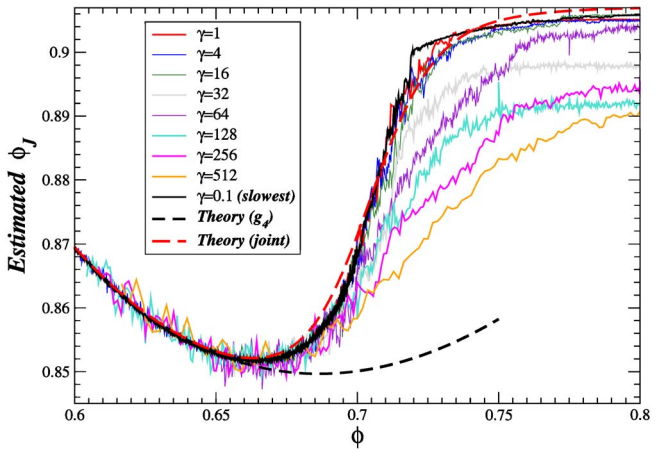

FIG. 2. (Color online) The equation of state for the monodisperse system of $N=4096$ hard disks, as is shown in Fig. 1 for hard spheres. Molecular dynamics runs are started with from isotropic liquid and the density increased slowly at different particle growth rates γ, as shown in units of 10^{-6} in the legend. The g_4 equation of state for the liquid [cf. Eq. (2) in Ref. 36] and the joint liquid-crystal EOS from Ref. 36 are also shown for comparison. It is seen that, for $\gamma<10^{-5}$, the system has sufficient time to equilibrate for all densities shown and the pressure closely follows the true equilibrium EOS (corresponding to the limit $\gamma\to 0$ and $N\to\infty$). We do not show the equivalent curves for runs starting with a perfect triangular crystal and decreasing the density (i.e., $\gamma<0$), since there is virtually no hysteresis observed from the EOS obtained by increasing the density.

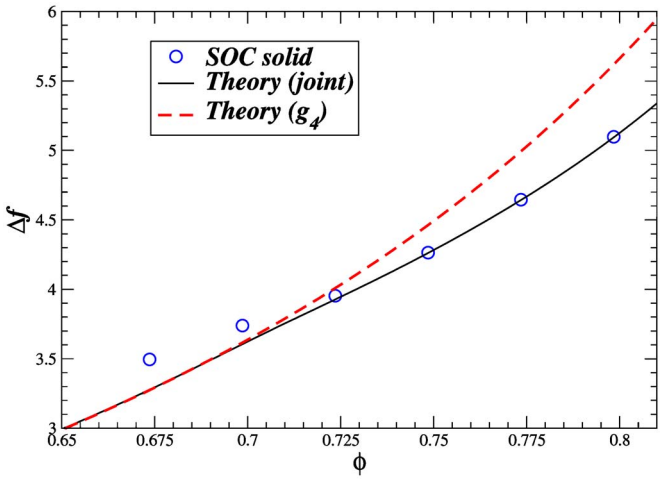

FIG. 3. (Color online) The excess free energy per particle Δf for a monodisperse system of hard disks, obtained through integration of the joint (global) liquid/solid EOS (Ref. 36), through the BCMD algorithm for SOC systems, and from the most accurate EOS from liquid-state theory (Ref. 36). It is seen that in the solid phase, $\phi>0.72$, the free energy of the SOC model closely matches that obtained by assuming a continuous EOS, demonstrating that the entropy jump between the liquid and solid phases at the transition is too small to be measured, if it exists at all (see also Fig. 13).

(as in the liquid state), the bounding cells are chosen to be sufficiently large to allow the system to explore the neighborhood of the metastable configuration freely, but are also sufficiently small to stabilize the structure of the metastable system and to prevent particle rearrangements. The free energy of this cell-constrained liquid is larger than that of the unconstrained liquid, which has more free volume available to explore, and it is hoped that the difference between the two is a good approximation to the configurational entropy for sufficiently high densities.

III. EQUILIBRIUM PHASE DIAGRAM

In this section, we use MD to determine the equation of state for monodisperse and bidisperse hard-disk systems and, also, to calculate the excess free energy per particle relative to the ideal gas at different densities. We use the MD data to estimate the location of the freezing transition in a binary hard-disk mixture. We predict that at a freezing density $\phi_F \approx 0.775$, a crystal of density $\phi\approx 0.8415$ composed of predominantly large particles should start precipitating from the liquid mixture. Our study here is similar to that carried out in significant detail for soft disks (interacting via an inverse 12th power potential).[34]

A. Monodisperse hard-disk systems

Whether the liquid-solid transition for the monodisperse hard-disk system is a continuous (second-order) transition or a discontinuous first-order transition is still disputed.[35] We will not try to resolve this question here. However, we must briefly examine the thermodynamics of monodisperse disks as this will be necessary in order to study mixtures. In Fig. 2, we show the EOS for monodisperse hard disks, obtained through molecular dynamics at different particle growth rates γ. A more detailed description of the procedure is in Sec. II A and an analogous plot for three dimensions is given in Fig. 1.

Unlike in three dimensions, there is no clear discontinuity between the EOS of the isotropic liquid and the triangular crystal. Slowing the rate of density increase allows us to find the true equilibrium EOS, as demonstrated by the fact that the observed EOS in Fig. 1 barely changes even though γ is decreased by more than an order of magnitude. The transition between the liquid and solid phases occurs in the density range $\phi\approx 0.69-0.72$, which would also be the best estimate for the coexistence region assuming that the transition is first order (the freezing density, in particular, can only be roughly estimated from the EOS curves alone). Even if the transition is first order, however, the change in entropy between the liquid and solid is very small and, therefore, for the purposes of free-energy calculations, we can assume that there is a continuous transition, i.e., that the free energy per particle $f_{\rm mono}(\phi)$ is a unique and smooth function of density. We will therefore not explicitly distinguish between the liquid and solid (and possible hexatic phase) of the monodisperse hard-disk system, but rather consider them as a single phase. This assumption will reduce the number of different phases to consider for mixtures and greatly simplify our calculations.

The numerical EOS $p_{\rm mono}(\phi)$ is well fitted by the semiempirical joint liquid-solid EOS proposed in Ref. 36. In Fig. 3, we show the free energy obtained by using the BCMD algorithm from Sec. II C with bounding cells of diameter twice larger than the diameter of the disks, i.e., $\Delta\mu=1$. For the crystal, the configurational entropy is identically zero and, therefore, the free-volume term is the only contribution to the thermodynamic free energy. Figure 3 shows that $f_{\rm mono}(\phi)$ is indeed (nearly) continuous when going from the liquid to the solid state. We note that one can avoid analytical

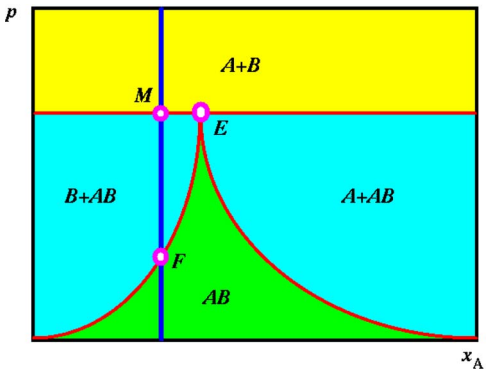

FIG. 4. (Color online) A schematic illustration of the eutectic phase diagram assumed to apply to binary mixtures of hard disks with dispersity $\kappa=1.4$. The monodisperse phases are denoted by A and B, and the liquid mixture by AB. The horizontal axes is the composition x_A, and the vertical axes is the pressure P. The location of the particular composition we study here is marked by a vertical line, along with the freezing point F, the melting point M, and the eutectic point E.

approximations completely and obtain $f_{\text{mono}}(\phi)$ numerically with high accuracy by simply integrating the numerical EOS from the low densities (where a low-order virial expansion is accurate), using the pressure from an MD simulation with sufficiently small γ.

B. Binary mixtures of hard disks

We study a binary mixture of disks with a one-third (composition $x_B=1/3$) of the disks having a diameter (size *dispersity*) $\kappa=1.4$ times larger than the remaining two-thirds ($x_A=2/3$).[8] Bidisperse disk packings with this aspect ratio and $x_A=x_B=1/2$ have been studied[70] as prototypical glass formers.[34] For this κ, it is believed that the high-density phase is a phase-separated crystal.[37] It can be proved that the highest density achievable with two disks of size ratio $\kappa<1.348$ is the same as for monodisperse disks, $\phi_{\max}=\pi/\sqrt{12}$,[38] although we are not aware of any proof that this highest density is only achievable in phase-separated configurations. For large size dispersity, denser packings exist where the small and large disks are mixed.[37,39] For small size dispersity, a substitutional triangular crystal, in which the large and small disks are randomly mixed, will be thermodynamically favored over the phase-separated crystal at intermediate densities because of its higher degeneracy entropy.[40,41] We will assume here that, for $\kappa=1.4$, the crystal phase is a phase-separated mixture of monodisperse triangular crystals and neglect any solubility of one type of disks into the crystal of the other type, since such solubility is expected to be negligible due to the large difference in size between the small and large disks.[41]

We also expect that the full (over all compositions) equilibrium phase diagram for this size dispersity will be of the eutectic type,[41] as schematically illustrated in Fig. 4. At low pressures, the equilibrium phase is a mixed isotropic liquid AB. Upon increasing the pressure, a freezing point is reached, and phase separation begins by precipitation of a monodispersed phase B composed of large particles, in mechanical equilibrium with the surrounding liquid AB (depleted in large particles). When the pressure exceeds the melting point, complete phase separation between the large and small disks occurs and the mixed liquid phase ceases to exist. It is important to note that the equilibrium phase diagram is typically presented at constant pressure and composition, whereas our simulations are carried out at constant volume and composition. For sufficiently large systems, the two ensembles must agree; however, for finite systems (we typically use $N=4096=64^2$ disks, 1365 large ones and 2731 small ones), coexistence is difficult to observe directly due to the surface tension between the coexisting phases.

The chemical potential in a monodisperse system is $\mu=f+p$, where f is the free energy per particle and p is the reduced pressure,[42] while the pressure is $P=p\phi/V_p$, where V_p is the volume of a particle and we have assumed that $k_BT=1$. The freezing point is the equilibrium point for phase B and phase AB at a given composition $x_A=1-x_B$. It can be determined by equating the (relative) chemical potential of particle type B inside the mixture AB, $\mu_{AB}^{(B)}$, with the chemical potential of the pure B phase, $\mu_B^{(B)}$, at equal pressures of the the two phases,

$$\mu_{AB}^{(B)}=\mu_B^{(B)},\qquad P_{AB}=P_B. \tag{4}$$

Carrying out several tedious calculations gives the following expressions for the required chemical potentials:

$$\mu_B^{(B)}(\phi_B)=\Delta f_B+p_B+\ln\phi_B-d\ln\kappa$$

$$\mu_{AB}^{(B)}(\phi_{AB})=\Delta f_{AB}+p_{AB}\frac{\kappa^d}{x_A+x_B\kappa^d}-x_A\tilde{\mu}_B+\ln\phi_{AB}$$
$$-x_A\frac{\kappa^d-1}{x_A+x_B\kappa^d}+\ln\frac{x_B}{x_A+x_B\kappa^d}.$$

Calculating the relative chemical potential $\mu_{AB}^{(B)}$ requires calculating the sensitivity of the excess free energy of the mixture with respect to the composition (at constant density)

$$\tilde{\mu}_B=\left(\frac{\partial\Delta f_{AB}}{\partial x_A}\right)_\phi,$$

in addition to the excess free energies and pressure at a fixed composition. This can be done numerically by calculating the excess free energy for mixtures with slightly differing compositions via thermodynamic integration starting at low densities (where a liquid theory approximate EOS works well enough). The condition of equal pressures gives

$$\pi=\frac{\phi_{AB}p_{AB}(\phi_{AB})}{x_A+x_B\kappa^d}=\frac{\phi_Bp_B(\phi_B)}{\kappa^d},$$

which can be used to express both ϕ_{AB} and ϕ_B as functions of π and then solve the equation $\mu_{AB}^{(B)}(\pi)=\mu_B^{(B)}(\pi)$ [cf. Eq. (4)].

We do not give the full details of this calculation here, and merely state the result for our binary mixture with $x_A=2/3$ and $\kappa=1.4$. Our free-energy calculations predict that, at densities higher than the freezing density $\phi_F\approx0.775$, a crystal of density $\phi\approx0.8415$ composed of predominantly large particles should start precipitating from the liquid mix-

ture (which remains at the freezing density). As we will see shortly, nucleation is kinetically strongly suppressed due to the need for large-scale diffusion of large disks toward the nucleus,[43] and, in fact, we have not observed spontaneous crystallization even in simulations lasting tens of millions of collisions per particle well above the estimated freezing density.

We note in passing that had we used the best theoretical liquid-state predictions for the EOS of the liquid mixture, as discussed in Ref. 36, instead of the numerical EOS, we would not predict a freezing transition at $\phi_F \approx 0.775$. Instead, at all pressures, the mixture would be predicted to be more stable, $\mu_{AB}^{(B)} < \mu_B^{(B)}$. As we will show in Sec. IV A, the liquid-state theoretical prediction for the EOS is not sufficiently accurate at the densities above $\phi \approx 0.75$. We are not aware of any better analytical form of the EOS for mixtures and, therefore, prefer to use an explicit numerical EOS for the liquid state. Also, note that predicting the melting point and eutectic points requires knowing the EOS for the liquid mixture at all compositions, and we have not tried to calculate them in this work as our focus is on the freezing transition and, in particular, the kinetic glass transition, at a fixed composition. In Ref. 34, an approximate EOS based on an effective single-component system was constructed, and the eutectic point was estimated to occur at a composition of $x_A = 0.75$. It is believed that mixtures closer to the eutectic composition are better glass formers, and this was one of our reasons for choosing a composition $x_A = 2/3$ instead of the commonly used $x_A = 1/2$.

The pair interaction potential used in Ref. 34 is of the inverse power form,

$$V_{ij}(r) = \epsilon \left(\frac{R_i + R_j}{r} \right)^n,$$

where R is the disk diameter and the exponent $n = 12$ is chosen. For such an interaction potential, all thermodynamic variables depend only on the scaled density

$$\tilde{\phi} = \left(\frac{\epsilon}{k_B T} \right)^{2/n} \phi,$$

where ϕ is the density (volume fraction) that a hard-disk system would have if the particle diameters are the same. In the limit $n \to \infty$, the interaction potential becomes that of the hard-disk system and $\tilde{\phi} = \phi$. For sufficiently large n, one expects that the behavior of the system, including melting and freezing points, will be close to the hard-disk limit. For a monodisperse disk system, the freezing point is known to be $\phi_F \approx 0.69$ for $n \to \infty$,[44] while for $n = 12$ it is $\phi_F \approx 0.763$.[34] The agreement is not perfect, but it encourages a comparison between our result for the freezing density of our mixture $\phi_F \approx 0.775$ (at $x_A = 0.67$) with that predicted to be the eutectic point in Ref. 34 (for $x_A = 0.75$). From the data given in that paper ($T^* = 0.54$, $\rho^* = 0.725$), we obtain $\tilde{\phi}_F \approx 0.761$, which is in reasonable agreement with our hard-disk result, when we take into account the different molar composition and the different interaction potential.

We briefly examine the phase-separated crystal $A+B$, which we call the *crystal* phase even though one of the monodisperse phases could, in fact, be liquid (i.e., not possess long-range translational order). If phase separation is complete, at a given overall density ϕ, the density of each of the phases $\phi_A(\phi)$ and $\phi_B(\phi)$ can be determined from the condition of mechanical equilibrium between the phases,

$$P = \frac{p_{\text{mono}}(\phi_A)\phi_A}{V_p^A} = \frac{p_{\text{mono}}(\phi_B)\phi_B}{V_p^B} = \frac{p_{\text{mono}}(\phi_B)\phi_B}{\kappa^d V_p^A},$$

along with the condition that the overall density be ϕ,

$$\frac{1}{\phi} = \frac{1}{x_A + x_B \kappa^d} \left(\frac{x_A}{\phi_A} + \frac{x_B \kappa^d}{\phi_B} \right).$$

The solution to these equations is shown in Fig. 5. It is seen that, at a given density, the phase B, composed of large particles, is at a higher density and, thus, higher reduced pressure. At a density of $\phi \approx 0.75$, the small-particle phase A melts to a liquid, i.e., loses its translational order.

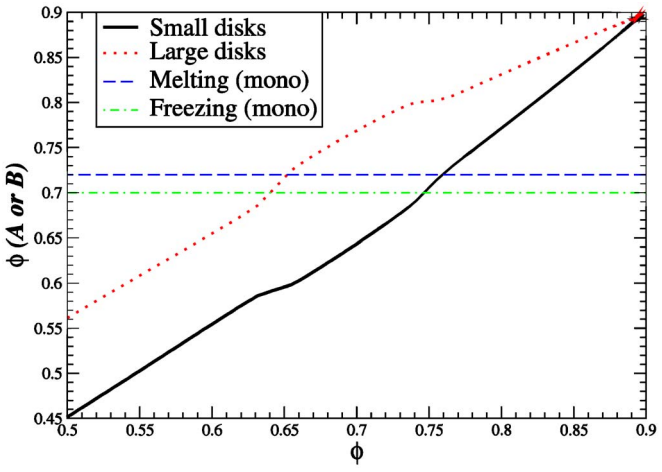

FIG. 5. (Color online) The densities $\phi_A(\phi)$ and $\phi_B(\phi)$ of the large- and small-particle phases in a fully phase-separated mixture at overall density ϕ. It is seen that the large-particle solid melts into a liquid at around $\phi \approx 0.75$, and at $\phi \approx 0.65$ the small-particle solid also melts. Note that this calculation assumes that there is no mixing between the small and large particles, which is only true at very high densities.

Below a certain density, the large particles should start diffusing into the phase of small particles, forming a mixture AB. We used molecular dynamics to observe this melting of the phase-separated crystal, starting from a high-density phase-separated mixture and reducing the density slowly. However, as Fig. 6 illustrates, even the slowest MD runs did not achieve true equilibrium, as seen by the strong dependence of the observed EOS on γ. It is seen that below a density of $\phi \approx 0.8$, the phase-separated crystal is no longer stable and large particles start diffusing in the small-particle phase. This diffusion is very slow and even tens of millions of collisions per particle cannot equilibrate the phase-separated systems properly. A similar observation was made for a binary mixture of soft disks in Ref. 34, and it was concluded that "heterogeneous simulations can no longer (below the glass transition temperature) help us to identify the thermodynamically stable phase." In our simulations, long MD runs at a fixed density observed complete melting at a density $\phi = 0.765$ and, therefore, it is clear that, at this density, the stable phase is the mixed liquid. However, at

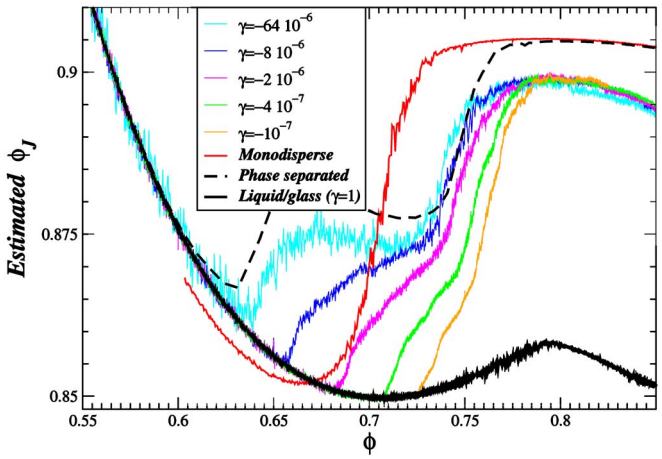

FIG. 6. (Color online) Equation of state as observed at different negative rates γ, starting from a phase-separated crystal. We also show the EOS obtained by compressing a dilute liquid with $\gamma=10^{-6}$, forming a glass at high densities. It is seen that the phase-separated samples fall out of equilibrium at densities below $\phi\approx 0.8$, when sluggish diffusion of large particles into the small-particle solid begins. At sufficiently low densities, complete melting into a mixed isotropic liquid occurs and the EOS matches the one measured by compressing a liquid. For comparison, we also show the EOS for the monodisperse hard-disk system from Fig. 2. Note that the EOS of the phase-separated crystal does not perfectly match that of the monodisperse crystal because of the finite-size effects coming from the interface between the large- and small-particle solids.

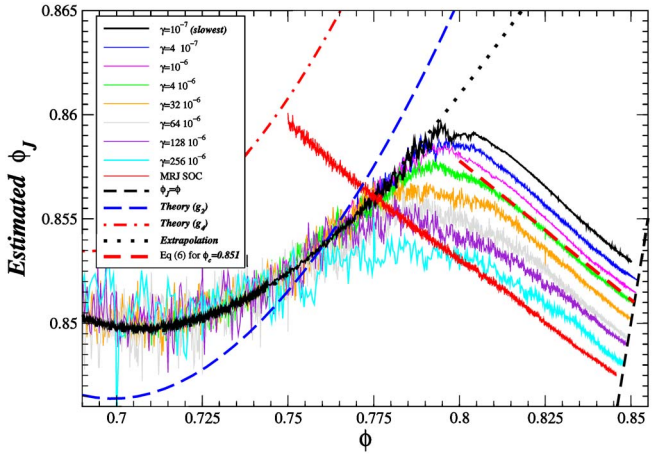

FIG. 7. (Color online) The equation of state $\tilde{\phi}_J(\phi)$ for $N=4096$ disks as observed by compressing a liquid with different expansion rates γ. At densities below $\phi\approx 0.775$, the runs at different expansion rates follow the EOS of the mixed liquid. However, after a kinetic glass transition density $\phi_g\approx 0.8$, the systems become trapped in glassy configurations even for the slowest runs. Note that we have run many more expansion rates over different density ranges and here we only show a representative sample. For comparison, we also show the theoretical liquid mixture EOS (Ref. 68), using either the Henderson (g_2) or improved (g_4) EOS for the monodisperse liquid, as given by Eq. (2) in Ref. 36. It is seen that the theoretical liquid theory prediction is not sufficiently accurate at these densities. The EOS for the SOC-constrained (estimated) MRJ glass is also shown.

$\phi=0.775$, only partial melting occurred and a crystallite of large particles remained stable for very long periods of time.

IV. IS THERE AN IDEAL BINARY DISK GLASS?

Theories and simulations have already cast doubt on the existence of ideal glass transitions in hard-particle systems.[8,23,45] For example, the slope of $s_c(\phi_J)$ at ϕ_J^{IG} dramatically affects the location of the presumed transition, and, in fact, an infinite slope shifts the transition to zero temperature.[46] Additionally, the validity of extrapolations into temperature/density regions that are inaccessible to accurate computer simulations,[47] as well as the importance of finite-size effects[48] have been questioned. We present a distinctly different evidence that the concept of an ideal glass transition is flawed. For our binary hard-disk system, we *explicitly* construct an exponential number of packings with jamming densities ϕ_J in the interval from the "amorphous" state, $\phi_J^g\approx 0.84$, to that of the phase-separated crystal, $\phi_{\max}=\pi/\sqrt{12}\approx 0.91$. This demonstrates that the configurational entropy is only zero for the crystal, rather than a hypothetical most-dense amorphous (ideal) glass.[8] A parallel critique of the concept of random close packing (RCP) was raised by one of us.[7] Specifically, there is a continuous trade-off between disorder (closely linked to degeneracy) and density, so that the concept of a most-dense random packing is ill defined. Instead, Ref. 7 replaces RCP with the maximally random jammed (MRJ) state, i.e., the most disordered of all jammed states.

A. Kinetic glass transition

The calculation of the true equilibrium liquid EOS is not possible inside the glassy region with conventional simulation methods, especially for large system sizes.[47–51] We produce glasses by starting with a low-density liquid and growing the particle diameters at a growth rate $\gamma\ll 1$,[11] for a very wide range of compression rates γ, as shown in Fig. 7. As seen in the figure, at densities below $\phi\approx 0.775$, the runs at different expansion rates are all in quasiequilibrium and follow approximately the same EOS, namely, the EOS of the isotropic mixed liquid. After this density, fast compressions fall out of equilibrium and follow a glassy EOS, leading to a disordered jammed packing. Up to a density of about $\phi_g\approx 0.8$, the slowest runs follow the same EOS, which suggests that this is the EOS of the supercompressed liquid, i.e., the metastable extension of the liquid branch.

This kind of liquid-branch extension cannot be obtained using MD for monodisperse spheres in three dimensions since slow compressions crystallize after the melting density is surpassed (cf. Fig. 1), and, therefore, theoretical predictions about the existence or analytical form of such a hypothetical branch[26,32] cannot be verified computationally. For the binary disk system, where crystallization does not occur, the results in Fig. 7 suggest that one can numerically study the liquid branch with high accuracy at least up to a density of $\phi_g\approx 0.8$. In order to analytically extend the liquid EOS beyond this density, we have fitted a cubic function to $\tilde{\phi}_J(\phi)$ for the slowest runs up to the density where slowing down the compression by an order of magnitude does not change the observed pressure (within statistical variability). The fit

$$\tilde{\phi}_J(\phi)=3.136-8.4826\phi+10.277\phi^2-4.0356\phi^3 \qquad (5)$$

is shown in Fig. 7. It should be emphasized that it is just a fit and there is no reason to believe that it is quantitatively accurate much beyond $\phi\approx 0.8$. It is important to point out

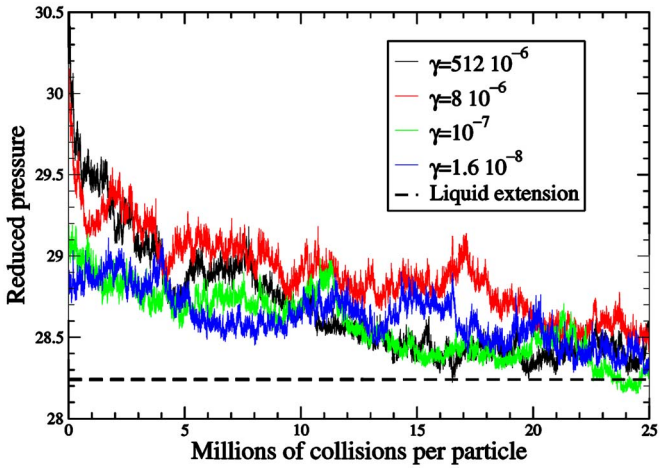

FIG. 8. (Color online) The relaxation of the pressure during long molecular runs at a fixed density $\phi=0.8$, for several of the glasses produced during the compressions shown in Fig. 7. For comparison, we show the pressure predicted by the liquid branch extension in Eq. (5).

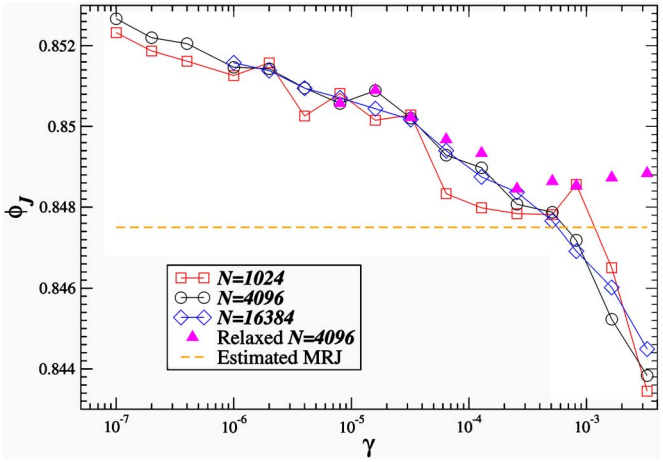

FIG. 9. (Color online) Final jamming density ϕ_J for different numbers of particles N, with and without additional relaxation (and subsequent slow compression) to ensure that a truly jammed packing has been reached.

that in order to prepare a system in an (metastable) equilibrium liquid configuration at such high densities, one must compress the (stable) liquid from lower density (at least $\phi \approx 0.75$) very slowly. Quenching the liquid fast to a high density produces states that are clearly not in any kind of thermodynamic equilibrium, even though they will appear metastable due to very large relaxation times.

As seen in Fig. 7, above the kinetic glass transition density $\phi_g \approx 0.8$, the systems become trapped in glassy configurations even for the slowest runs and jam in disordered packings with jamming densities $\phi_J \approx 0.85$. Note that different definitions can be used for what the glass transition density is. Here, we take it to be the maximal density at which our simulations can equilibrate (not necessarily in the true equilibrium state, but at least in a metastable liquid state) the binary mixtures. We also see in Fig. 7 that the nonequilibrium glassy EOS is very well described by an empirical linear relation,

$$\tilde{\phi}_J = (1+\alpha)\phi_J - \alpha\phi, \tag{6}$$

where $\alpha \approx 0.133$, over a wide range of $\phi > \phi_g$. We do not yet have a theoretical understanding of this relation.

It is clear from the figure that even the slowest compressions fall out of equilibrium at a density around ϕ_g, so that equilibrating the liquid in reasonable time is not possible beyond this kinetic glass transition density. Very long MD runs, with as many as 50×10^6 collisions per particle, have failed to equilibrate our samples at a fixed $\phi=0.8$, and, in fact, very different microstructures all remained stationary for very long periods of time. This is shown in Fig. 8, where we show the evolution of the pressure during long molecular dynamics runs at $\phi=0.8$ for several of the states in Fig. 7, at fixed density. For the glasses produced with faster expansion rates, the initial pressure is higher and then decays more rapidly. However, a very slow residual decay of the pressure is seen in all of the samples, indicating the occurrence of very slow structural relaxation.

The final jamming densities of the glasses compressed at different rates are shown in Fig. 9. Note that slower compressions consistently yield denser packings with no hints of the existence of a *densest* glass. Fast compressions produce packings that are not truly jammed[11] and subsequent relaxation of these systems increases the density to around $\phi_J \approx 0.847$. This behavior of our hard-disk systems is closely related to the observation that supercooled liquids sample saddle points with the saddle index vanishing only below the temperature where even the slowest cooling schedules fall out of equilibrium,[15,52] i.e., the kinetic glass transition temperature. Observations similar to those in in Fig. 9 have already been made for systems of soft particles, e.g., the lowest energy of the sampled inherent structures has been shown to continuously decrease for slower cooling.[5]

In Fig. 10, we show the EOS for the SOC-constrained solids obtained by taking a snapshot of a liquid configuration at densities ranging from 0.7 (well within the equilibrated

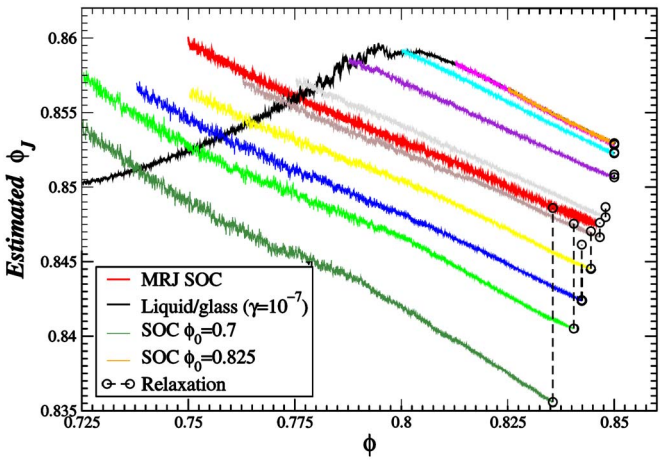

FIG. 10. (Color online) The EOS for SOC solids obtained by bounding each disk within a cell of twice its size, starting with liquid or glass configurations generated by saving snapshot configurations during one of the slowest compression shown in Fig. 7 ($\gamma=10^{-7}$, replicated from Fig. 7 for comparison) and then compressing the SOC solid at $\gamma=10^{-6}$ to near jamming. The initial densities ϕ_0 go from 0.7 to 0.825 and in the legend we only mark the first and last curves since ϕ_0 can be read from the starting point of the each curve. Also shown is the relaxation of the pressure (i.e., increase in ϕ_J) after the cell constraints are removed.

liquid density range) to 0.825 (well within the out-of-equilibrium glassy density range), and enclosing it with a bounding cell with $\Delta\mu=1$. The liquid/glass configurations were generated by saving snapshot configurations during the slowest compression shown in Fig. 7 ($\gamma=10^{-7}$). In the SOC models, we measure the reduced pressure p through the momentum exchange during interparticle collisions only, and do not include the pressure on the walls of the cells p_c. The SOC solid has a lower pressure than the unconstrained liquid because of the presence of cells, and the difference between the two diminishes as the density increases, becoming virtually negligible beyond the kinetic glass transition density. It is interesting to observe that the EOS of the SOC solids also follows Eq. (6) closely. The compressions of the SOC solids generated from liquid snapshots seem to produce jammed packings at densities as low as $\phi_J\approx 0.83$. However, these packings are unstable once the bounding cells are removed and molecular dynamics is run at a constant density, as shown in Fig. 7. In particular, this subsequent relaxation leads to glasses with $\phi_J\approx 0.85$, which is our best estimate for the MRJ density, as discussed in more detail shortly.

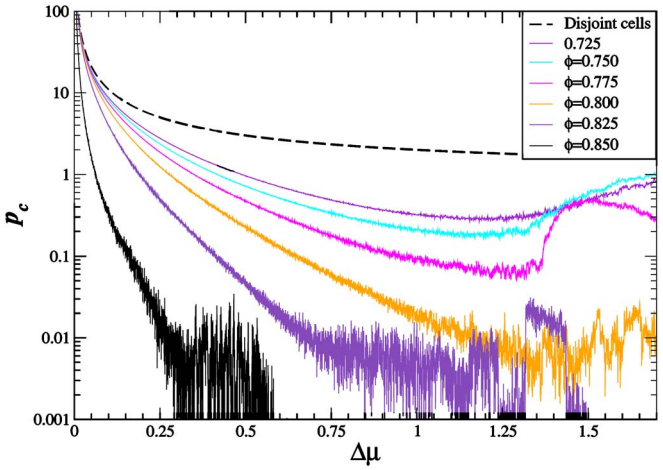

FIG. 11. (Color online) The averaged pressure on the bounding cell walls $p_c(\Delta\mu)$ as a function of the size of the cells for SOC glasses at several different densities. Qualitatively similar results are shown in Ref. 69. For comparison, the cell pressure that would be measured if the bounding cells are disjoint is shown. Note that when p_c becomes very small the simulation is not able to measure it accurately within the time interval over which particle-cell collisional momentum transfer is averaged.

B. Configurational entropy of glasses

In this section, we focus on calculating the free-volume and configurational contributions to the entropy of the dense liquid and glassy states obtained by compressing a liquid at different rates γ.

The number of jammed packings with jamming density ϕ_J, $N_g(\phi_J)=\exp[Ns_c(\phi_J)]$, was recently estimated for binary mixtures of relatively small numbers of hard disks via explicit enumeration.[53] An approximately Gaussian $N_g(\phi_J)$ was observed that is peaked at a density $\phi_{\mathrm{MRJ}}\approx 0.842$, interpreted to correspond to the MRJ state for this system. A Gaussian $N_g(\phi_J)$, corresponding to an inverted parabola for $s_c(\phi_J)$, is usually assumed as a first guess.[27] For large systems, explicit enumeration of all of the jammed packings is not yet possible. Instead, thermodynamics has been used to estimate $s_c(\phi_J)$ as the difference between the entropy (per particle) of the liquid $s_L(\phi)$ and the entropy of the "glass" $s_g(\phi)$,

$$s_c[\hat{\phi}_J(\phi)]=s_L(\phi)-s_g(\phi). \tag{7}$$

The liquid entropy s_L is obtained via thermodynamic integration of the *equilibrium* liquid EOS from the ideal-gas limit. Here, we use the numerical EOS as obtained from various small compressions (i.e., the smallest γ we have been able to use) as an estimate for s_L. The glass entropy s_g is defined as the entropy of the system constrained to vibrate around a single basin with jamming density ϕ_J, without the possibility of particle rearrangements. In the truly glassy region, the system is typically spontaneously constrained (jammed) by virtue of a very slow rearrangement dynamics, so that s_g can be defined reasonably precisely. For dense liquids, however, there is significant ambiguity in defining the constraints bounding a single jamming basin.

Formally, one can always partition configuration space into disjoint basins, each basin centered around a jammed configuration. For soft spheres such a partitioning can be defined by associating with each energy minimum (inherent structure) the basin of states for which gradient descent leads to the energy minimum under consideration. Such a partition is only useful, however, if the configurational volume (free energy) of a given basin $s_g(\phi,\phi_J)$ can be estimated easily, so that the number of basins can be calculated from Eq. (7). Note that the number of basins can only be estimated using thermodynamics up to exponential factors in N. We define the glass free-volume entropy $f_g=-s_g$ as the free energy of the SOC-constrained glass, where the cell is sufficiently large so that the pressure on the cell walls p_c is negligible, and small enough to prevent particle rearrangements.[71] The measured f_g obviously depends on the chosen bounding cell scaling (relative to the particles) $1+\Delta\mu_{\max}$, unless the pressure on the cell walls $p_c(\Delta\mu)$ decays sufficiently rapidly so that truncating its integral at a given $\Delta\mu_{\max}$ does not substantially increase the free energy.

In Fig. 11, we show $p_c(\Delta\mu)$ for SOC-constrained glasses at several different densities (as in Fig. 10, but this time shrinking the bounding cells rather than growing the particles). We see that at densities above the kinetic glass transition, within numerical accuracy, $p_c(\Delta\mu)$ goes to zero as $\Delta\mu$ increases. However, for densities below the kinetic glass transition $p_c(\Delta\mu)$ clearly remains positive and, therefore, the f_g measured for the SOC glass will show significant dependence on the choice of cell cutoff. Here, we choose the cutoff to correspond to the (shallow) minimum in $p_c(\Delta\mu)$, if there is a minimum, or the point at which $p_c(\Delta\mu)$ becomes numerically indistinguishable from zero [$p_c(\Delta\mu)<0.01$ in Fig. 11] otherwise. Closely related methods have previously been used to calculate s_c.[28,31,54] For soft-particle glasses, an alternative method is to use the harmonic approximation to the vibrational entropy at an energy minimum as an estimate of s_g.[29,30] All methods are rigorous only in the jamming or $T\to 0$ limit and are approximate for truly equilibrated liquids, so our quantitative results at low ϕ should be interpreted with caution.

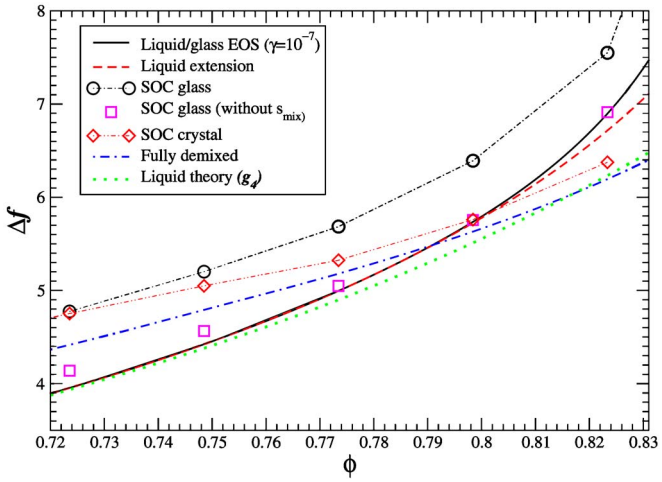

FIG. 12. (Color online) The excess free energy of the compressed liquid/glass phase (with and without s_{mix}), and of phase-separated SOC-constrained crystals (note that the cell constraints prevent mixing at any density). The quantitative results for glasses at low densities ($\phi<0.8$) should be interpreted with caution. Also shown are the predictions for an ideal phase-separated mixture, which does not perfectly match with that of the SOC solids even at high densities because of the entropic cost of the interface between the large- and small-particle solids.

The excess free energy of the SOC glassy mixtures is shown in Fig. 12, along with the free energy of the most-equilibrated liquid/glass $f_L(\phi)$ obtained by integrating the numerical EOS from the ideal-gas limit. We see that the free energy of the SOC glasses is substantially higher than that of the unconstrained liquid at all densities. However, the difference becomes approximately constant at high densities and seems to approach the entropy of mixing $s_{\mathrm{mix}}=x_A \ln x_A + x_B \ln x_B \approx 0.6365$. With this observation in mind, we show the measured $s_c(\phi)=s_L(\phi)-s_g(\phi)$ for the different glass compressions in Fig. 13. For comparison, the results for a slow compression of a monodisperse system are also shown, and the entropy of mixing has been subtracted from s_c. It is seen that, for the monodisperse case, s_c-s_{mix} ($s_{\mathrm{mix}}=0$ in this case) becomes very nearly zero after the liquid freezes (around $\phi\approx 0.7$), indicating a continuous or a very mildly discontinuous liquid-solid phase transition (see also Fig. 3).

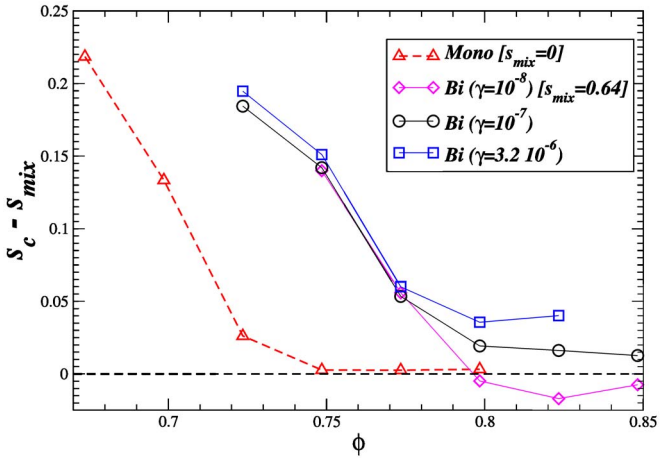

FIG. 13. (Color online) Estimated $s_c(\phi)-s_{\mathrm{mix}}$ for monodisperse and bidisperse systems of $N=4096$ disks, as obtained from (sufficiently slow) compressions with a range of γ's. The quantiative results for glasses at low densities ($\phi<0.8$) should be interpreted with caution.

More interesting is the fact that s_c-s_{mix} also becomes nearly zero for the binary glasses around the kinetic phase transition (around $\phi\approx 0.8$). This important observation has not been made before. It means that the estimated number of packings that the liquid samples near the glass transition is very close to s_{mix}, which is also the entropy of the uncorrelated ensemble of discrete states in which a fraction x_A of the particles is chosen to be large and the remaining particles are chosen to be small. It is interesting to observe that the parabolic fit to $s_c(\phi_J)$ from the work in Ref. 53, if constrained to equal the mixing entropy at the maximum, passes through zero at $\phi\approx 0.9$, much higher than the extrapolation in Ref. 27 and close to the crystal jamming density. We note that all measurements of s_c in the literature that we are aware of are above or close to s_c near the kinetic glass transition, and all estimates of the zero crossing of s_c are based on extrapolations beyond this point without numerical support.[27–32]

C. Microsegregated glasses

The observations made in Fig. 13 strongly suggest that extrapolations of s_c above the kinetic transition, predicting an ideal glass transition at density below the maximal possible density, are flawed. The only way to get zero configurational entropy is to get rid of the entropy of mixing, i.e., to fully demix the two types of disks. In fact, an exponential number of amorphous jammed packings exist over the whole density range from that accepted as the MRJ density $\phi_{\mathrm{MRJ}}\approx 0.84$ to that of the phase-separated crystal $\phi_{\max}\approx 0.91$. Lower-density jammed packings also exist;[53] however, they do not have thermodynamic significance and, thus, our simulations do not generate them. In our simulations, we observe that higher ϕ_J implies microsegregation in the form of increased clustering of the large particles. This has been most vividly demonstrated in Ref. 34. This observation suggests that one can generate denser packings by artificially encouraging clustering, i.e., increasing the amount of (spatial) ordering in the packings.

We employ the following procedure in order to encourage clustering of disks of the same size: We perform molecular dynamics starting from a monodisperse ($\kappa=1$) triangular crystal at pressure $p=100$ in which a third of the particles has been selected as being "large." These selected particles then slowly grow in diameter while the pressure tensor is maintained isotropic and constant using a Parinello-Rahman-type variation of the MD algorithm.[19] The growth of the large particles changes the size ratio κ, and, when $\kappa=1.4$, we stop the process and then slowly compress the system to a very high pressure (jamming). We can achieve a desired level of clustering and higher jamming densities for the final packings by spatially biasing the initial partitioning into large and small disks. Figure 14 illustrates two different jammed packings, one with an uncorrelated random choice of large disks and another with correlations encouraging microsegregation. The packing produced by an uncorrelated random assign-

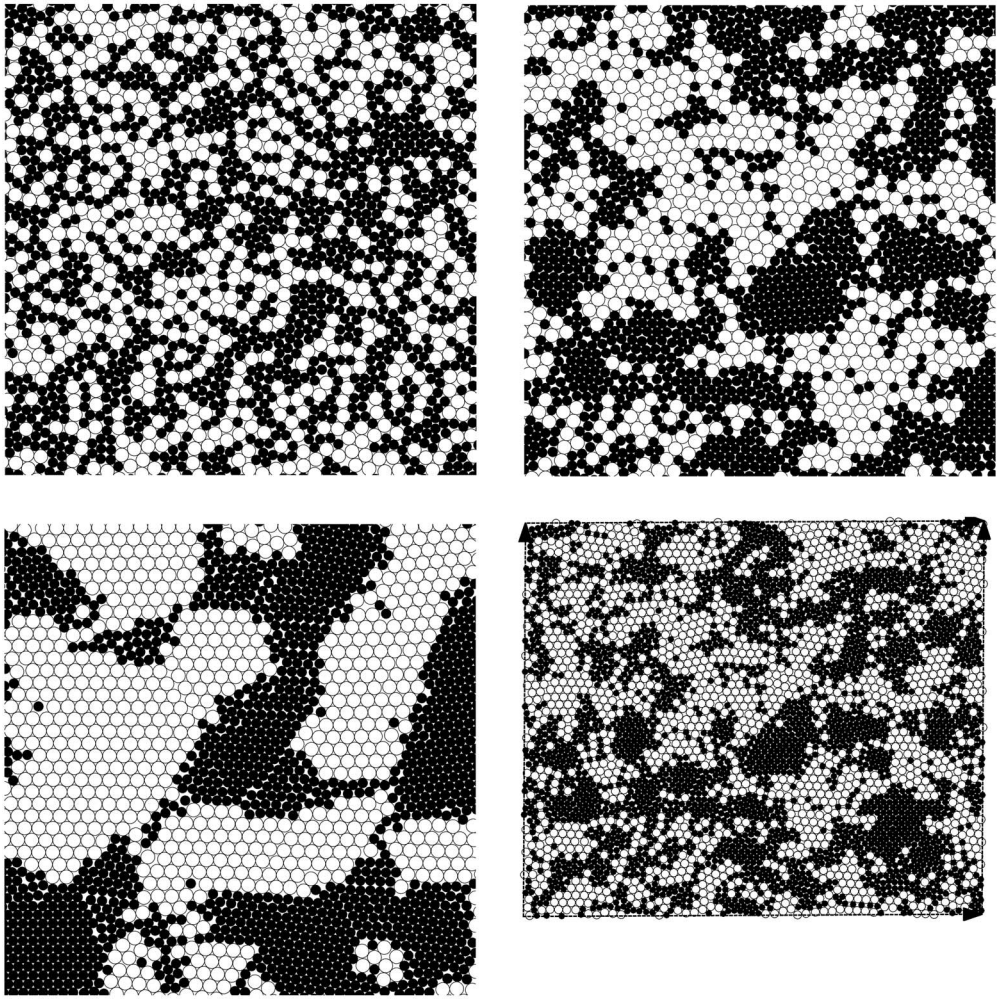

FIG. 14. The microstructure of a packing without significant clustering (top left, $\phi_J \approx \phi_{\mathrm{MRJ}} \approx 0.846$, $R=1$, and $\nu=0.1$), with moderate clustering (top right, $\phi_J \approx 0.850$, $R=1$, and $\nu=1.0$), and with strong clustering (bottom left, $\phi_J \approx 0.865$, $R=2$, and $\nu=2.0$). For better visualization, we only show portions of the simulated system. For comparison, we show the full-size packing ($N=4096$) with moderate clustering in the bottom right inset. The lattice vectors of the periodic unit cell are also shown. The unit cell started as a square, however, it deformed to a rectangular shape during the MD algorithm (even more so for stronger initial clustering).

ment of small versus large particles is the most disordered packing, i.e., it is representative of the MRJ state for this binary hard-disk mixtures.

For the purpose of creating clustered initial assignments of small or large (i.e., A or B) labels, we use a level-cut of a Gaussian random field (GRF).[55] Specifically, we construct a discretized GRF on a square lattice of $4096=64^2$,[56] and assign label A to all sites where the field has value larger than a certain cutoff (chosen so that two-thirds of the disks are labeled A), and label B otherwise. By using suitably chosen parameters for a flexible family of pair correlation functions originally proposed by Matern,[57] we were able to generate different levels of clustering, as illustrated in the inset in Fig. 16. Specifically, the two parameters for the Matern correlation are the correlation length R and the interface smoothness parameter $0<\nu<1$. Increasing R or ν increases the clustering, and we used five values of R going from 1 to 5, along with five values of ν going from 0.1 to 0.5, for a total of 25 different types of microsegregated initial configurations. Higher values of R and ν produce denser packings as the B disks are grown in size at constant pressure, as illustrated in Fig. 15.

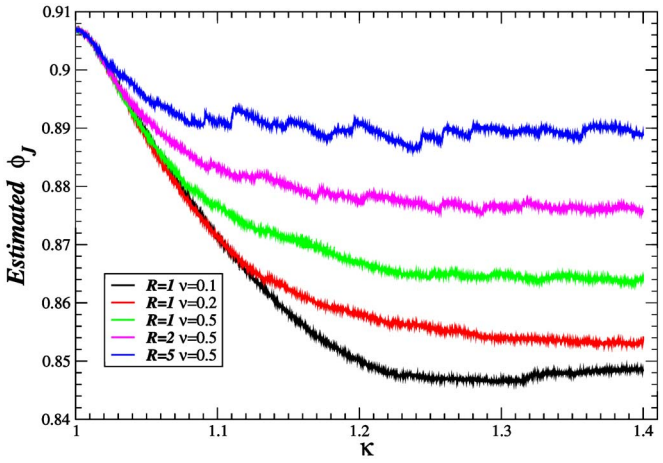

FIG. 15. (Color online) Converting an initially monodisperse disk packing of $N=4096$ disks into a jammed binary disk packing by slowly growing a chosen third of the disks at a growth rate $\gamma=10^{-5}$ while keeping the pressure at $p \approx 100$. Here, we used a leveled GRF with the Matern correlation in order to generate clustered initial configuration. It is seen that the estimated jamming density $\tilde{\phi}_J(\kappa)$ decreases from $\tilde{\phi}_J \approx 0.91$ as the size dispersity κ grows to the final value of $\kappa=1.4$. The larger the final jamming density, the more clustered the initial configuration is.

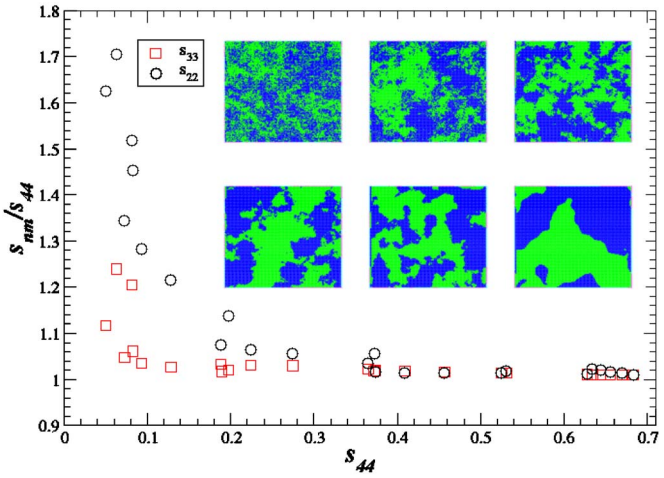

FIG. 16. (Color online) The Markov approximation $s_{n,n}$ to the entropy per site for $n=2-4$ (Ref. 58), for different choices of the parameters R and ν for the Matern correlation function in the GRF. It is seen that $s_{3,3}$ is close to $s_{4,4}$, suggesting that $s_{4,4}$ is a good approximation to the true entropy per site, especially for less clustered configurations (i.e., higher $s_{4,4}$). (Inset) Sample realizations of the partitioning into large and small sites on a 64^2 grid, for several values of R and ν.

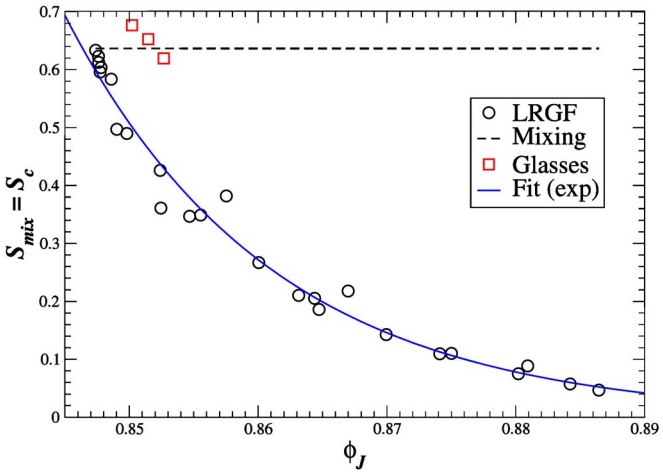

FIG. 17. (Color online) The measured degeneracy of packings of $N=4096$ disks obtained by using different parameters of a random Gaussian field with Matern correlations (Ref. 55), as a function of the jamming density. For comparison, we have shown $s_c(\phi=0.825)$ for the three glass compressions shown in Fig. 13, and an exponential fit to the data.

To determine the configurational entropy (degeneracy) for a given choice of the GRF parameters, we use a recently developed algorithm for obtaining numerical approximations of the entropy (per site) of lattice systems.[58] In principle, the true degeneracy can be calculated by measuring the probability $p(\mathcal{C})$ of observing a particular configuration $\mathcal{C}$ of a rectangular window of $n\times m$ sites, and then calculating the entropy per site

$$s_{n,m}=\lim_{n,m\to\infty}\frac{S_{n,m}}{nm}=\lim_{n,m\to\infty}\left\{-\frac{1}{nm}\sum_{C}[p(\mathcal{C})\ln p(\mathcal{C})]\right\},$$

where the sum is over all of the possible 2^{nm} configurations. The above limit is approximated accurately and efficiently with small windows by exploiting a Markov approximation,[58] to obtain

$$s_{n,m}\approx S_{n,m}-S_{n-1,m}-S_{n,m-1}+S_{n-1,m-1}.$$

This approximation is seen to converge relatively fast, as demonstrated in Fig. 16 for the 25 different choices of parameters R and ν for the Matern correlation function. We have used windows of 4×4 sites, since calculating $S_{n,m}$ requires generating many GRFs for the same correlation function and counting the probabilities of observing different configurations of a window of size $n\times m$ sites. This process becomes prohibitively expensive for $n=m=5$.

We will assume that a different assignment of A and B labels will produce a distinct jammed packing, i.e., that the set of packings produced by the use of our procedure with a particular GRF forms a subset of all of the distinct jammed packings. Furthermore, we assume that the configurational entropy s_c for the jammed packings generated with a particular choice of GRF is well approximated by $s_{n,n}$ for sufficiently large n (we use $s_{4,4}$ from Fig. 16). In light of these approximations, the s_c we have calculated is a *lower bound* on the true configurational entropy of the binary hard-disk system. Figure 17 shows our results for s_c versus the jamming density ϕ_J, for the 25 different choices of the GRF parameters. The results clearly show that, in order to increase ϕ_J, one must sacrifice degeneracy (i.e., decrease s_c). The figure also shows the first *measured*, rather than extrapolated, estimate of $s_c(\phi_J)$. This observed $s_c(\phi_J)$ only goes to zero for the phase-separated crystal state, rather than the hypothetical amorphous ideal glass state postulated by extrapolations.

It is not *a priori* obvious that $s_c(R,\nu)$ is strongly correlated with $\phi_J(R,\nu)$, since they both depend on both R and ν. Such a strong correlation is demonstrated to be the case in Fig. 18, where we show color plots of $s_c(R,\nu)$ and $\phi_J(R,\nu)$ over the grid of 25 values for (R,ν). This strong correlation may be due to the particular choice of the correlation function in the GRF; however, it seems that such a trade-off between density and disorder is inevitable. Ideally, what we are interested in thermodynamically is the highest s_c at a given ϕ_J, i.e., the type of microclustering that decreases the degeneracy the least in order to increase the jamming density by a given amount from ϕ_{MRJ}. We do not know how to calculate the true $s_c(\phi_J)$ or how to construct samples representative of the most disordered samples at densities other than ϕ_{MRJ}. The results obtained for the particular way we generated microsegregated samples, shown in Fig. 17, show a rapid drop in s_c away from the MRJ point. That is, one must cluster significantly before seeing an appreciable increase in the jamming density.

A calculation of f_J for the different microsegregated glasses, using the BCMD algorithm, shows that f_J is essentially constant independent of (R,ν), at least to within statistical fluctuations. Substituting this in Eq. (3) together with the exponential fit $s_c(\phi_J)$ from Fig. 17 predicts that, for densities lower than $\phi\approx0.8$, the equilibrated liquid samples the MRJ basin, $\hat{\phi}_J(\phi)=\phi_{\mathrm{MRJ}}$, and for higher densities, the liquid samples the phase-separated crystal basin, $\hat{\phi}_J(\phi)=\phi_{\max}$. On the other hand, the smoothly increasing $\phi_J(\gamma)$ in Fig. 9, the spontaneous clustering seen for supercooled soft disks in Ref. 34, and the widely observed lowering of the energies of the sampled inherent structures for soft-sphere glasses upon

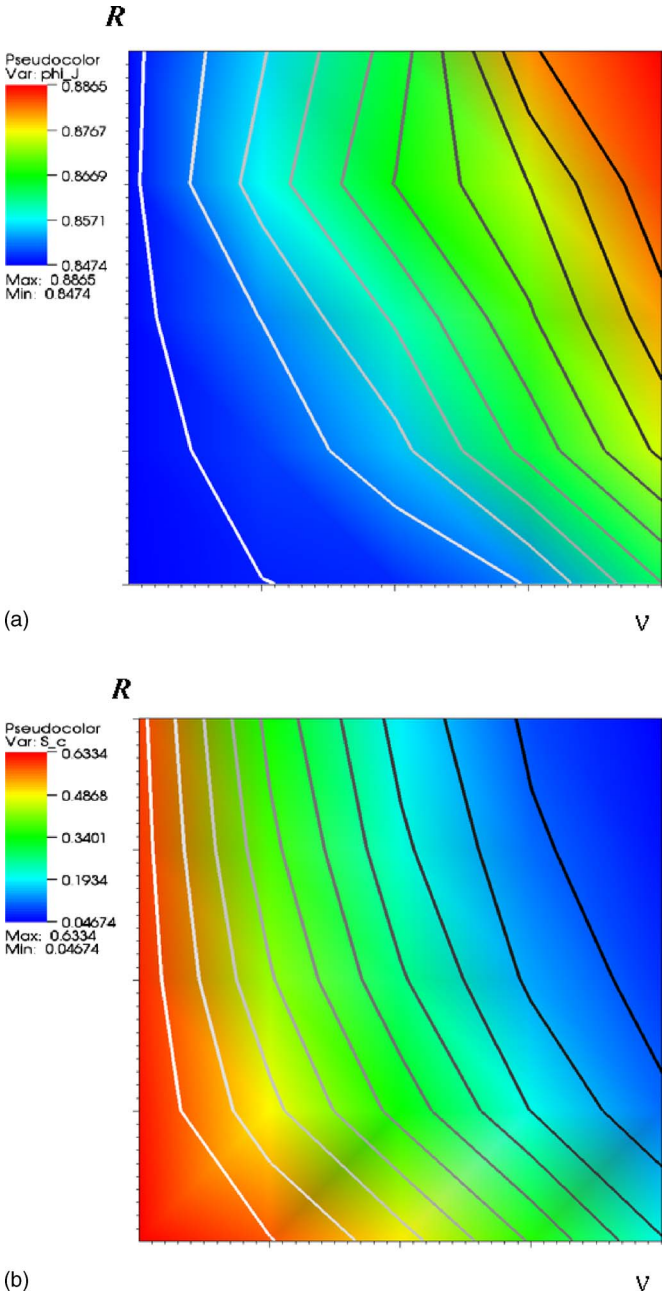

FIG. 18. (Color online) A demonstration that $s_c(R,\nu)$ (b) is strongly correlated with $\phi_J(R,\nu)$ (a). The x axes of the color plots is ν, and the y axes is R. If a similarly strong correlation exists for different choices of clustering correlations, it is important to determine whether the $s_c(\phi_J)$ we show in Fig. 17 applies to other choices of GRFs.

supercooling[5] all suggest that $\hat{\phi}_J(\phi)$ should be continuously increasing for very dense liquids. Such behavior of $\hat{\phi}_J(\phi)$, at least within the inherent-structure formalism we consider here, requires that $s_c(\phi_J)$ decay very slowly around ϕ_{MRJ}, so that the liquid prefers to lose degeneracy by ordering (clustering) in order to gain free volume. We expect that there exists an exponential number of ordered jammed states with densities lower than ϕ_{MRJ}, and, therefore, that $s_c(\phi_J)$ is a smooth function, rather than having a cusplike maximum or sharp discontinuity at ϕ_{MRJ}. In fact, the expected behavior in $s_c(\phi_J)$ is that it would be quadratic around ϕ_{MRJ}, i.e., close to an inverted parabola with a maximum at ϕ_{MRJ}.

V. CONCLUSIONS

In this paper, we studied a binary hard-disk system as a prototypical glass former. We explicitly demonstrated that the concept of random close packing (RCP) as the most-dense jammed amorphous packing is flawed, continuing on work in Ref. 7. We constructed an exponential number of amorphous jammed packings with densities spanning the range from the most disordered to most ordered jammed states. This simple yet powerful construction continually trades off degeneracy for density. We explicitly calculated, rather than extrapolated, the degeneracy entropy for densities well above that of the postulated ideal glass transition. We found that the degeneracy is positive for all "amorphous" states and is very close to the mixing entropy for the maximally random jammed state. Furthermore, the configurational entropy vanishes only for the phase-separated crystal. Free-energy calculations predicted a thermodynamic crystallization well below the kinetic glass transition. This points to the fact that the glass is metastable even for binary mixtures and casts additional doubt on the search for a thermodynamic origin of the glass transition.

It is important to stress that our argument has nothing to do with mixing macroscopic liquid and crystal domains (with sharp and identifiable interfaces that make for a negligible reduction in density) in order to get mixed states of intermediate densities. Instead, we construct an exponential number of amorphous configurations that show no signs of crystal nuclei. Artificially mixing large crystal domains with large liquid domains severely underestimates the number of available jamming configurations, since, in the vicinity of the glass transition, the configurational entropy is close to the entropy of the completely mixed system. For the binary hard-disk system, there is no sharp boundary between crystal and liquid states. The microseparated samples we constructed in our work are not mixtures of a liquid and a crystal phase. They are disordered (amorphous) states that have no qualitative difference from the liquid state. In particular, they do not have (quasi)long-range order and do not have macroscopic domains that could be considered crystal. Perhaps more significantly, these states are not artificial constructions in which we just mixed some crystal and liquid in a trivial manner. Rather, our choice was motivated by careful observations of the actual thermodynamic and kinetic behavior of hard-disk mixtures. Specifically, as we decreased the compression rate (cooling rate for soft disks), we saw spontaneous microclustering happening (this has been observed in other systems). If we had many more decades of computational power, we believe we would see microsegregated glassy states appear spontaneously.

Unfortunately, our results do not resolve the mystery of the nature of the glass transition. In fact, the complete thermodynamic behavior of hard-disk mixtures remains unclear. Free-energy calculations predicted a freezing transition, but it could not be observed directly with classical MD due to the dramatic kinetic slowdown near the glass transition. Such free-energy calculations proceed in reverse order: One assumes what are the equilibrium structures, and then selects the one with the lowest free energy. At high densities, how-

ever, it is not clear what are the properties of the liquid phase, and whether it exists at all. It is hoped that the inherent-structure formalism, i.e., the partitioning of the available configuration space into jamming basins, can describe the thermodynamic properties of dense or cool liquids well. For hard-sphere systems, this requires the identification and counting of distinct configurations in a statistical ensemble of jammed packings. This has been done by direct enumeration for small systems, however, enumeration is not possible for large systems. In this work, we identified distinct packings for hard-disk mixtures with distinct partitionings of the disks in a monodisperse triangular crystal into small and large disks. Such an identification converts the difficult geometrical problem of packing disks into a much simpler combinatorial problem of generating partitionings of the triangular lattice. This identification was suggested by the fact that the calculated configurational entropy near the glass transition is very close to the mixing entropy.

For the purposes of calculating configurational entropy, it is not necessary that the identification is one to one. Rather, it is only necessary that the number of jammed packings corresponding to a given partitioning (and vice versa) is subexponential in N, or exponential in N but with a multiplier that is small compared to the multiplicity of the partitioning. Starting with a given partitioning, we described a procedure for generating a corresponding packing using MD. While it is not trivial to prove mathematically that this generates a unique and distinct packing, we expect that this would be the case if the MD algorithm would be run for an infinitely long time at infinite pressure. In the other direction, starting with a given jammed isostatic bidisperse packing, one can shrink the diameters of the large particles and maintain the existing contacts, while also maintaining jamming. Along the way, new contacts will be formed and old contacts broken, and the path of the algorithm is not unique, but it is expected that the number of different choices that can be made is subexponential in N. In the end, this procedure will generate a monodisperse jammed packing in which the otherwise identical disks are labeled either small or large. Our previous analysis[59] suggested that the majority of strictly jammed monodisperse disk packings are the triangular packings with vacancies. These arguments suggest that for hard-disk mixtures there may indeed be a strong correspondence between jammed packings and partitionings of the triangular lattice. It would be a useful future exercises to consider adding vacancies to the initial triangular configurations before applying the Gaussian random fields to them. This might increase $s_c(\phi)$ and produce the expected inverted parabolic shape and, in particular, generate jammed packings at densities below ϕ_{MRJ}.

We believe that the fundamental principles are general enough to be applicable to a host of related systems, notably, both mono- and bidisperse with hard-core and soft interactions. Specifically, in all of these systems there will be an exponential number of states in between the most disordered (most amorphous) and most-ordered (crystal) one. For binary mixtures of soft disks the partially segregated configurations we constructed will correspond to inherent structures with continually decreasing depths. Similar constructions to the one used here (starting with microsegregated lattice configurations to obtain denser amorphous packings) can be carried out for three-dimensional binary mixtures as well. However, the computational effort involved in preparing sufficiently large samples and calculating their configurational entropy explicitly will be significantly higher. Furthermore, simulations of dense or supercooled liquids in three dimensions are more computationally demanding and the quasiequilibrium behavior of overcompressed or supercooled binary mixtures has not yet been clearly determined. It is therefore difficult to guess the structure of the dense glasses; we expect that microsegregation will occur even in three dimensions, but the increase in dimensionality also increases the number of available ways to arrange the particles in order to reduce the free energy.

The existence of an ideal glass transition for monodisperse hard-sphere systems remains an open question. It should be noted that *monodisperse* systems in both two and three dimensions are arguably *not* good model systems for the study of the glass transition. Hard-disk systems crystallize very easily and do not seem to form disordered jammed packings,[59] and hard-sphere systems crystallize relatively easily and therefore highly nonequilibrium protocols with unknown effects are needed in order to suppress crystallization and produce glasses.[7] Nevertheless, we have not yet identified an explicit construction of an exponential number of monodisperse jammed packings with densities spanning the range from 0.64 to 0.74. Such a construction is necessary in order to convincingly demonstrate that the configurational entropy is only zero for perfect crystals and thus refute theoretical models suggesting the existence of an ideal glass transition in dimensions higher than two.[60,61] These and related issues are discussed in more detail in Ref. 61, where it is, however, assumed that one can define a most-dense RCP, contrary to our results for both binary hard-disk mixtures and monodisperse spheres.

Finally, one should keep in mind that the binary hard-disk mixture is a *prototypical* glass former and therefore any successful theory of the glass transition should also apply to it. It should also be noted that we refuted only one (albeit popular) possible thermodynamic origin of the glass transition (specifically, vanishing of the configurational entropy) and that there may be other possibilities. Recent work has developed detailed thermodynamic theories of glassy states in certain systems,[62] including binary hard-disk mixtures.[63,64] It is found that, similarly to what we find for binary hard-disk mixtures, there is no sharp thermodynamic glass transition (at positive temperature). Rather, these works find a continuous decrease in the number of configurations that the system explores as the temperature is lowered, becoming very small, but still positive, near the observed kinetic glass transition. This suggests an Adams-Gibbs-type formula for the relaxation time which however does not diverge at some ideal transition. Extrapolations or approximate theories based on the observed behavior in the liquid region above the kinetic transition would have wrongly predicted an ideal glass transition in such systems. This shows that predicting the true thermodynamic behavior of very dense or supercooled systems requires complex statistical mechanics calculations

that, to our knowledge, can explicitly be carried out only for model systems in two dimensions. Future theoretical and computational work will hopefully be able to treat three-dimensional systems.

An important avenue of research is the development of algorithms to equilibrate liquids at densities higher than the kinetic glass transition. It is clear that such algorithms must be very different from classical MD. However, despite the fact that several algorithms have helped significantly reduce the simulation times necessary to equilibrate supercooled or super-compressed liquids,[47–51] true thermodynamic (meta) equilibrium for samples of reasonable size has not yet been achieved at sufficiently high densities to properly elucidate the thermodynamics of disordered solids. Finally, the continued failure to identify any thermodynamic origin to the glass transition suggests that the kinetics of supercooled and supercompressed liquids needs to be understood better. We believe that the hard-sphere system is an ideal model for such studies.

ACKNOWLEDGMENTS

This work was supported in part by the National Science Foundation under Grant No. DMS-0312067.

[1] J. Jackle, Rep. Prog. Phys. **49**, 171 (1986).
[2] R. Zallen, *The Physics of Amorphous Solids* (Wiley, New York, 1983).
[3] J. D. Bernal, *Liquids: Structure, Properties, Solid Interactions*, edited by T. J. Hughel (Elsevier, New York, 1965), pp. 25–50.
[4] G. Adam and J. H. Gibbs, J. Chem. Phys. **43**, 139 (1965).
[5] P. G. Debenedetti and F. H. Stillinger, Nature (London) **410**, 259 (2001).
[6] F. Sciortino, J. Stat. Mech.: Theory Exp. 2005, P05015.
[7] S. Torquato, T. M. Truskett, and P. G. Debenedetti, Phys. Rev. Lett. **84**, 2064 (2000).
[8] A. Donev, F. H. Stillinger, and S. Torquato, Phys. Rev. Lett. **96**, 225502 (2006).
[9] M. P. Allen, G. T. Evans, D. Frenkel, and B. M. Mulder, Adv. Chem. Phys. **86**, 1 (1993).
[10] F. H. Stillinger and T. A. Weber, J. Chem. Phys. **83**, 4767 (1985).
[11] A. Donev, S. Torquato, and F. H. Stillinger, Phys. Rev. E **71**, 011105 (2005).
[12] A. Donev, S. Torquato, F. H. Stillinger, and R. Connelly, J. Comput. Phys. **197**, 139 (2004).
[13] C. S. O'Hern, E. Silbert, A. J. Liu, and S. R. Nagel, Phys. Rev. E **68**, 011306 (2003).
[14] A. Donev, S. Torquato, F. H. Stillinger, and R. Connelly, Phys. Rev. E **70**, 043301 (2004).
[15] M. S. Shell, P. G. Debenedetti, and A. Z. Panagiotopoulos, Phys. Rev. Lett. **92**, 035506 (2004).
[16] A. Donev, Ph.D. thesis, Princeton University, 2006, available at http://cherrypit.princeton.edu/donev.
[17] B. D. Lubachevsky and F. H. Stillinger, J. Stat. Phys. **60**, 561 (1990).
[18] B. D. Lubachevsky, F. H. Stillinger, and E. N. Pinson, J. Stat. Phys. **64**, 501 (1991).
[19] A. Donev, S. Torquato, and F. H. Stillinger, J. Comput. Phys. **202**, 737 (2005).
[20] A. Donev, R. Connelly, F. H. Stillinger, and S. Torquato, Phys. Rev. E **75**, 051304 (2007).
[21] S. Torquato and F. H. Stillinger, J. Phys. Chem. B **105**, 11849 (2001); see also S. Torquato, A. Donev, and F. H. Stillinger, Int. J. Solids Struct. **40**, 7143 (2003).
[22] Z. W. Salsburg and W. W. Wood, J. Chem. Phys. **37**, 798 (1962).
[23] M. D. Rintoul and S. Torquato, Phys. Rev. Lett. **77**, 4198 (1996).
[24] M. D. Rintoul and S. Torquato, J. Chem. Phys. **105**, 9258 (1996).
[25] A. Donev, F. H. Stillinger, and S. Torquato, J. Comput. Phys. **225**, 5095 (2007).
[26] R. J. Speedy, Mol. Phys. **95**, 169 (1998).
[27] R. J. Speedy, J. Chem. Phys. **110**, 4559 (1999).
[28] S. Sastry, J. Phys.: Condens. Matter **12**, 6515 (2000).
[29] F. Sciortino, W. Kob, and P. Tartaglia, Phys. Rev. Lett. **83**, 3214 (1999).
[30] B. Coluzzi, G. Parisi, and P. Verrocchio, Phys. Rev. Lett. **84**, 306 (2000).
[31] L. Angelani, G. Foffi, and F. Sciortino, e-print arXiv:cond-mat/0506447.
[32] G. Parisi and F. Zamponi, J. Chem. Phys. **123**, 144501 (2005).
[33] L. V. Woodcock, Faraday Discuss. **106**, 325 (1997).
[34] D. N. Perera and P. Harrowell, Phys. Rev. E **59**, 5721 (1999).
[35] H. Weber, D. Marx, and K. Binder, Phys. Rev. B **51**, 14636 (1995).
[36] S. Luding, Phys. Rev. E **63**, 042201 (2001).
[37] C. N. Likos and C. L. Henley, Philos. Mag. B **68**, 85 (1993).
[38] T. Kennedy, arXiv:math/0412418.
[39] O. Ouche, F. H. Stillinger, and S. Torquato, Physica A **342**, 428 (2004).
[40] X. C. Zeng, D. W. Oxtoby, and Y. Rosenfeld, Phys. Rev. A **43**, 2064 (1991).
[41] R. J. Wheatley, Mol. Phys. **93**, 965 (1998).
[42] D. Frenkel and B. Smit, *Understanding Molecular Simulation* (Academic, New York, 2002).
[43] S. R. Williams, I. K. Snook, and W. van Megen, Phys. Rev. E **64**, 021506 (2001).
[44] W. G. Hoover and F. H. Ree, J. Chem. Phys. **49**, 3609 (1968).
[45] W. Krauth, Nature (London) **405**, 550 (2000).
[46] P. G. Debenedetti, M. S. Shell, and F. H. Stillinger, J. Phys. Chem. B **107**, 14434 (2003).
[47] Q. Yan, T. S. Jain, and J. J. de Pablo, Phys. Rev. Lett. **92**, 235701 (2004).
[48] Y. Brumer and D. R. Reichman, J. Phys. Chem. B **108**, 6832 (2004).
[49] T. S. Grigera and G. Parisi, Phys. Rev. E **63**, 045102(R) (2001).
[50] L. A. Fernandez, V. Martin-Mayor, and P. Verrocchio, Philos. Mag. **87**, 581 (2007).
[51] K. K. Bhattacharya and J. P. Sethna, Phys. Rev. E **57**, 2553 (1998).
[52] T. S. Grigera, A. Cavagna, I. Giardina, and G. Parisi, Phys. Rev. Lett. **88**, 055502 (2002).
[53] N. Xu, J. Blawzdziewicz, and C. O'Hern, Phys. Rev. E **71**, 061306 (2005).
[54] R. J. Speedy, J. Chem. Phys. **114**, 9069 (2001).
[55] S. Marčelja, Physica A **231**, 168 (1996).
[56] B. Kozintsev and B. Kedem, J. Comput. Graph. Stat. **9**, 286 (2000); Software for GAUSSIAN package is at http://www.math.umd.edu/~bnk/CLIP/clip.gauss.htm
[57] B. Matern, *Spatial Variation*, Lecture Notes in Statistics Vol. 36 (Springer Verlag, Berlin, 1960).
[58] P. Attard, in *Statistical Physics on the Eve of the Twenty-First Century* (World Scientific, Singapore, 1999).
[59] A. Donev, S. Torquato, F. H. Stillinger, and R. Connelly, J. Appl. Phys. **95**, 989 (2004).
[60] F. Zamponi, Philos. Mag. **87**, 485 (2007).
[61] F. Zamponi, Phys. Rev. E **75**, 043101 (2007).
[62] V. Ilyin, E. Lerner, T.-S. Lo, and I. Procaccia (to be published) (2007).
[63] E. Aharonov, E. Bouchbinder, H. G. E. Hentschel, V. Ilyin, N. Makedonska, I. Procaccia, and N. Schupper, Europhys. Lett. **77**, 56002 (2007).
[64] H. G. E. Hentschel, V. Ilyin, N. Makedonska, I. Procaccia, and N. Schupper, Phys. Rev. E **75**, 050404 (2007).
[65] R. J. Speedy, J. Phys.: Condens. Matter **9**, 8591 (1997).
[66] R. J. Speedy, J. Phys.: Condens. Matter **10**, 4387 (1998).
[67] J. K. Percus and G. J. Yevick, Phys. Rev. **110**, 1 (1958).
[68] S. Luding and A. Santos, J. Chem. Phys. **121**, 8458 (2004).
[69] R. J. Speedy, Mol. Phys. **80**, 1105 (1993).
[70] Our choice of composition is closer to the estimated eutectic point for disk mixtures with $\kappa=1.4$[34] than the commonly used $x_A=x_B=1/2$ and also leads to equal area fractions of the large and small disks.
[71] We have found that $\Delta\mu=1$, i.e., a cell diameter twice the diameter of the disk it bounds, is sufficiently small to prevent particle rearrangements, see Fig. 11.